Hindawi
Journal of Advanced Transportation
Volume 2020, Article ID 9689604, 14 pages
https://doi.org/10.1155/2020/9689604

Research Article

Multirotor Sizing Methodology with Flight Time Estimation

Marcin Biczyski,[1] **Rabia Sehab**,[1] **James F. Whidborne**,[2] **Guillaume Krebs**,[3] **and Patrick Luk**[4]

[1]*On-Board Energies and Systems Division, ESTACA Campus West, 53000 Laval, France*
[2]*Centre for Aeronautics, Cranfield University, MK43 0AL Cranfield, UK*
[3]*Pôle "Systèmes" ECo2, GeePs - CentraleSupelec, 91192 Gif sur Yvette, France*
[4]*Electric Power and Drives Group, Cranfield University, MK43 0AL Cranfield, UK*

Correspondence should be addressed to Marcin Biczyski; marcin.biczyski@estaca.fr

Received 26 July 2019; Accepted 15 October 2019; Published 20 January 2020

Guest Editor: Umberto Papa

Copyright © 2020 Marcin Biczyski et al. This is an open access article distributed under the Creative Commons Attribution License, which permits unrestricted use, distribution, and reproduction in any medium, provided the original work is properly cited.

This paper addresses the need for sizing of rotors for multirotor vehicle applications such as personal air transport, delivery, surveillance, and photography. A methodology for the propeller and motor selection is developed and augmented with flight time estimation capabilities. Being multirotor-specific it makes use of the platform's simplicity to rapidly provide a set of off-the-shelf components ready to be used in the vehicle. Use of operating points makes the comparison process fast, precise, and tailored to specific application. The method is easily implemented in software to provide an automated tool. Furthermore, clearly defined input and output parameters make it also usable as a module in other multicriteria optimisation algorithms. The new methodology is validated through comparison with a consumer-grade drone and the calculated results are compliant with manufacturer's specification in terms of maximum hover time.

1. Introduction

In recent years, Unmanned Aerial Vehicles (UAVs) have become a popular solution for a variety of civil and military applications including surveillance, photo- and videography, and land surveying. The versatility of these systems has even found them in many nonstandard purposes such as automated package delivery or Personal Air Vehicles (PAVs). Multirotor UAV platforms have gained particular attention due to their Vertical Take Off and Landing (VTOL) capabilities as well as their simple construction and control. Of paramount importance is safety and reliability, especially when it comes to autonomous solutions, and so the enterprise market offers complete, closed drone solutions at different size/weight points. These are simple-to-use systems with a high degree of user support and good performance for most applications. However, the mechanical simplicity of the platform means that customized and open solutions should be available for specialized applications. Furthermore, the main limitation of multirotor systems is their flight time, mostly due to battery weight and energy storage constraints. Therefore, a set of tools needs to be created that can aid the design of customized solutions that can be specifically tailored for a particular application. Thus there is a need for a methodology to automatically select the best consumer-grade components to build a custom solution at a given weight and performance level.

There are some methodologies in the open literature for this purpose, but few lead directly to a "bill-of-materials" level solution. The most popular approach to obtaining a "flyable" configuration seems to be to test various *motor + propeller* combinations and choose one that suits the application [1]. Although popular with hobbyists, the method has little value in the commercial or research environment due to high cost (purchase of components), time requirement, and the need for specialized equipment (thrust stand, dynamometer). This method provides the most accurate results, but the number of combinations needed to be tested increases geometrically with each added component. This process can be significantly sped up using calculators such as Drive Calculator [2] and eCalc [3], which incorporate some of the data in their databases, but still the selection needs to be performed manually. This lack of search automatization capability and weak interfacing with other software (e.g., MATLAB) renders it difficult when analysing more than one case. In addition, eCalc does not pay that much attention to the main lifting body – the propeller, and uses a mathematical model (diameter and pitch can be input manually) for the performance calculation, as opposed to a more accurate database of measured/simulated data. Therefore,

alternative methods can still be proposed that improve accuracy, versatility or usability of database-driven approach.

Multirotor-specific methodologies have been developed by Gatti and Giulietti [4], Gatti [5] and Kim et al. [6]. They all used statistical methods to estimate relations between different components of the propulsion chain. The first two use analytical methods from the area of aerospace to calculate take-off weight based on mission requirements, and the last manages to simplify the drone propulsion model to a single equation to obtain generated power or thrust. Unfortunately, these approaches provide too little data to properly size the components, and in some cases even require the data of a selected component to work. Therefore, while useful for calculating the target multirotor weight for the application, they cannot be used for the component selection process.

Although not solving the problem completely, there are several methods that help with the preliminary multirotor design. Basset et al. [7] present past and current efforts to develop UAV presizing methodologies. They focus on conceptual, as well as numerical aspects of the vehicle. Due to the confidential nature of the projects, the paper does not go into much detail of the inner workings of the methodologies. However, most of them share a trait of being as general as possible in order to make them applicable to every configuration, which is not desired when dealing with an already chosen topology, such as multirotor, due to possible oversimplification and loss of optimisation opportunities.

A detailed database-free multirotor sizing methodology has been presented by Bershadsky et al. [8], that has been implemented in a tool called Electric Multirotor Sizing Tool (EMST). The authors have shown its versatility and accuracy with several examples. Unfortunately, their parametric approach requires heavy generalisation of component models, that keeps the mean error low, but may lead to significant errors for more unusual configurations. Yet, the authors have demonstrated award-winning results even for very tight constraints. However, it should still be possible to achieve a similar level of accuracy with alternative methods, with the added benefits of reduced computational cost and increased flexibility through decreased number of dependencies in the system.

Dai et al. [9] have addressed a very important issue, that is often neglected in other texts – the selection of components that best match calculated parameters. The proposed methodology divides the sizing problem into twelve sub-problems: eight of them optimise weight and efficiency of the components and the remainder four try to best match a real component to the calculated optimised parameters. Unfortunately, this degree of compartmentalization has the disadvantage that the real product parameters do not affect the optimisation process and this restricts the opportunity for further improvement of the design. It is especially important, as in a more recent paper [10] the authors focus on the role of propeller optimisation and the importance of propeller and motor coupling.

A different approach was taken by Magnussen et al. [11] who treated the propulsion system sizing problem as a mixed-integer programming problem. The strengths of this method are a solid definition of the base problem and the ability to use external solvers. However, the user still needs to provide the data of considered components. The added value of this



Figure 1: Multirotor in *quad X* configuration with visible components of the propulsion chain. (i) Flight Controller, (ii) ESC (under arm), (iii) BLDC Motor, (iv) propeller, and (v) battery connector.

methodology is the ability to model the dynamic motor thrust response, which is a useful tool for dynamic performance analysis. However, for basic sizing applications the complexity (up to 3091 variables in the example problem) may be too overwhelming and a simpler solution may be preferred.

This paper presents a method for sizing of the multirotor propulsion system through the selection of propeller and motor. Furthermore, the method provides the necessary data for the selection of the Electronic Speed Controller (ESC) and battery. Additionally, it gives a way of comparing different configurations through estimation of flight time by modelling battery discharge at constant power requirement. The key point of the methodology is the fact that it works on real components (propellers and motors) increasing the precision of the estimation. Another feature is the ability for the selection process to be automated making it an useful module for use in novel optimisation algorithms. Elements of optimisation are included in order to provide efficient and feasible solution. However, it should be noted that the resultant configuration is based on estimations, assumptions and inaccurate data, and therefore not optimal, so the methodology results should be treated only as a *good first guess*.

The paper is structured as follows; Section 2 details all the elements of the multirotor propulsion chain and their interaction; Section 3 describes the methodology based on the inverted model from the previous section; Section 4 presents example results for a small drone such as DJI Phantom 4 V2.0 and extends the findings onto Personal Air Vehicles; finally, Section 5 concludes the paper and highlights the most important outcomes.

2. Multirotor Propulsion Chain

Multirotors as a category of flying vehicles cover a lot of variants differing not only in the number of rotors, but also their placement. Currently, the most popular configuration

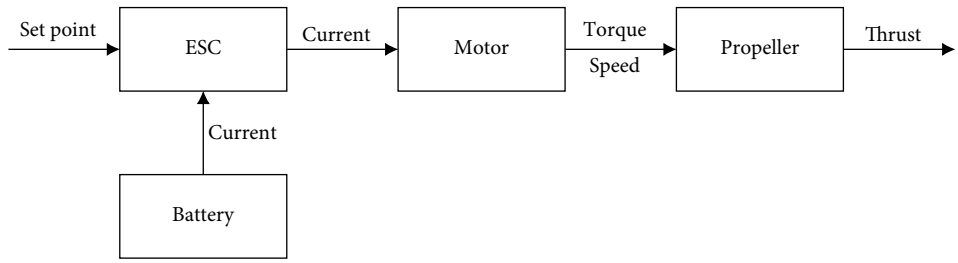


Figure 2: Multirotor propulsion chain diagram.

seems to be *quad X* with four parallel rotors placed diagonally from the center, as shown in Figure 1. One of the characteristic properties of most multirotors is their symmetry and the fact that every arm is the same, except for the rotor spinning direction. This makes it easy to analyse the propulsion system for the general case by analysing only one arm (one propulsion chain). The Flight Controller (FC) is responsible for control strategy for the whole platform and preparing a set point for each arm, but it does not participate in the propulsion chain as such.

In most cases, Brushless DC (BLDC) motors are used for multirotor propulsion, but sometimes, usually for toys under 100 g, DC motors are also used. This paper focuses only on BLDC; however, most concepts shown apply to both types. Brushless motors do not have physical brushes, so they require Electronic Speed Controllers (ESC) to achieve electronic commutation. Therefore, the main components of the propulsion chain are identified to be: *propeller*, *motor*, *ESC,* and *battery*. A schematic of the propulsion model of a multirotor is shown in Figure 2. It can be seen that there is one input of a set point (given by FC) and one output, namely the thrust generated by the propeller. Therefore, the propulsion chain can be identified as a open-loop Single Input Single Output (SISO) system, which makes it relatively easy to size components one at a time. In the next part of this section, each component will be described in detail.

2.1. Propeller. Aircraft propellers are characterized by 3 main parameters: diameter, pitch, and the number of blades. Generally, the higher these are, the higher the thrust generated, but also higher torque is exerted on the motor. However, long, slowly spinning, 2-bladed propellers are known to be more aerodynamically efficient than small, fast-spinning, multibladed ones. Propeller characteristics are mainly a function of its rotational speed and the speed of incoming air. However, if we consider air density to be constant and the air to be static (at hover in still air), the thrust, torque, and power depend only on propeller speed. Additionally, there are secondary parameters such as mass and geometry template expressed as manufacturing series (e.g., Multirotor, Slow Flyer, Carbon, etc.).

2.2. Motor. In a multirotor, the motor's main objective is to drive the propeller reliably and with high acceleration, so the speed can be changed quickly. The main limitations of a BLDC motor are in terms of speed and current. Maximum current is often stated by the manufacturer and maximum speed in no-load conditions ω_0 can be calculated from the KV parameter multiplied by the applied voltage V:

$$\omega_0 = \mathrm{KV} \times V. \tag{1}$$

With a constant voltage, when current is applied, the motor starts exerting torque on the shaft accelerating it until its torque equals the load torque, assuming the mechanical losses are neglected. At low speed, far from the motor constraints, it is assumed that the relation between motor torque and current is constant and expressed with motor torque constant (K_T). Therefore, the applied current is transformed into the torque based on the motor characteristic, then the torque is transformed into speed based on the propeller torque–speed characteristic, and finally the speed is transformed into thrust using the propeller thrust–speed characteristic. This sequence makes the propulsion chain easy to calculate analytically as a SISO system.

2.3. Electronic Speed Controller. Although Electronic Speed Controllers (ESCs) serve a very important purpose in the real-life multirotor, in the propulsion chain model it has very little importance. In the model, its function is reduced to transferring current from the battery to the motor under constant voltage. However, when designing a multirotor, ESC still needs to be sized according to the maximum current flowing to the motor.

2.4. Battery. When it comes to lightweight aerial vehicles, Lithium Polymer (LiPo) batteries currently dominate the market due to their high energy density and high current discharge capabilities [5, 12]. These batteries are composed of several cells connected in series (rarely in parallel). Cell voltage changes according to the state of charge with 4.2 V being at 100%, 3.85 V at 50% and 3.7 V (nominal) at 20%. However, discharging a LiPo cell under 3 V leads to permanent damage to the battery. Therefore, it is recommended to only discharge the batteries to about 20%, which grants a Depth of Discharge (DoD) of 80%. The cells can be connected in series or in parallel, denoted by *S* or *P,* respectively, so for example, 4*S*1*P* is a 4 cell battery with 14.8 V nominal voltage. Additionally, the batteries are characterized by their capacity in mAh and a C-rating (r_C), which specifies the maximum current that can be drawn continuously, for example 35 C × 5.2 Ah = 182 A (the unit being C and not Coulomb). It is evident that maximum discharge current is not dependent on battery capacity.

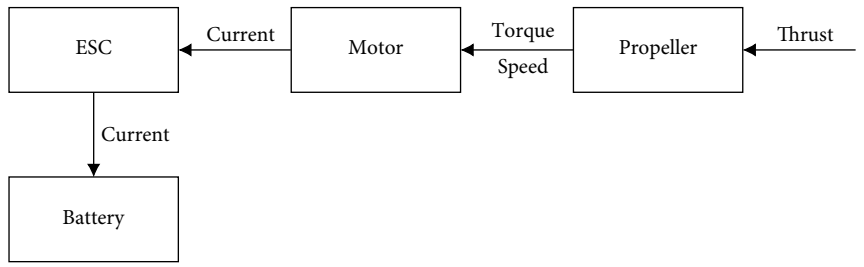


Figure 3: Inverted multirotor propulsion chain diagram.

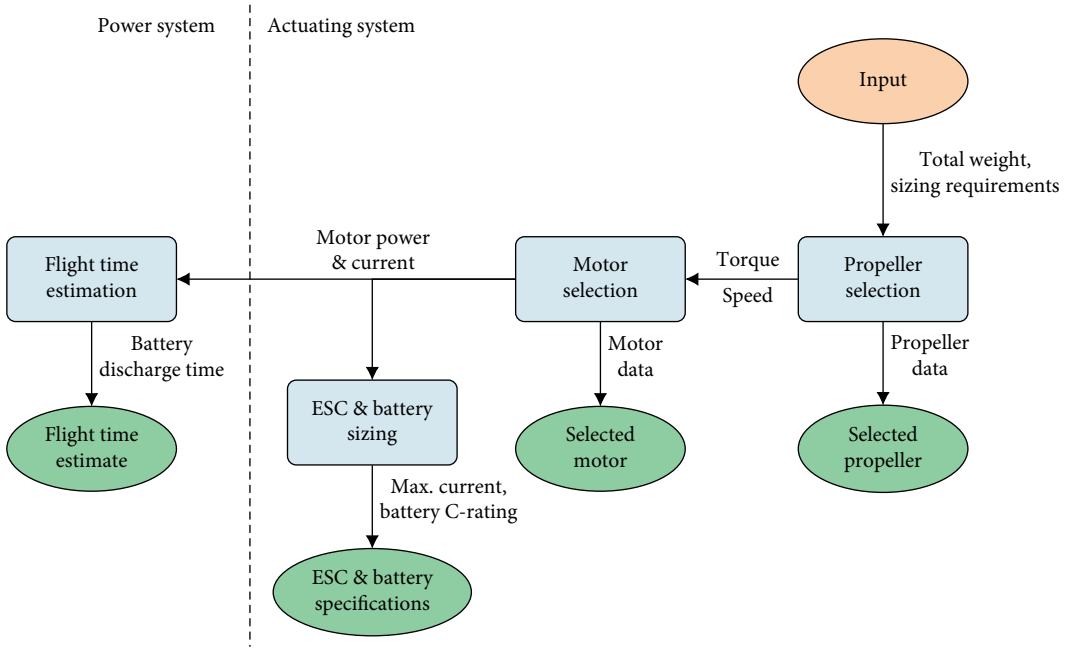


Figure 4: Simplified sizing methodology flowchart with division into two sub-systems.

3. Sizing Methodology

By inverting the propulsion system model developed in the previous section, a new model can be obtained allowing to estimate battery voltage based on thrust generated, as shown in Figure 3. This allows for an iterative approach in order to determine the time required to deplete the battery at constant power draw, which effectively serves as a flight time estimate. Thus, two distinct subsystems can be distinguished in the system model: the actuating system and the power system. This manifests itself in the sizing methodology, which is also divided into two parts. Figure 4 shows a simplified view of the methodology. Although it is based on the diagram in Figure 3, it also shows the separation between battery sizing and battery simulation (flight time simulation).

3.1. Actuating System. The actuating system provides the thrust propulsion to the vehicle and consists of the propeller, the motor, an ESC to control the motor and a battery to power the motor. The propeller sizing and selection is performed first, the motor sizing being dependent on the propeller properties. Finally, specifications for the ESC and the battery are produced.

The propulsion system model used here is only applicable in static conditions and at constant speed. Modelling a multirotor in flight is much more complicated due to the presence of aerodynamic effects such as variable angle of attack, reduction of thrust coefficient with advance ratio, and additional frame drag. However, an approximation of the required performance for full controllability in flight is made using the model only in static conditions of operation. It uses a state of equilibrium achieved at hover (in no-wind conditions), where thrust generated by the propellers is equal to the multirotor's weight. This thrust can be multiplied by a constant thrust-to-weight ratio to achieve a value of static thrust that guarantees specific performance in the air depending on the application. This approach appears imprecise; however, during the years of use of similar methods in the community of radio controlled aircraft modellers, the values of thrust-to-weight ratio required for different applications have been validated with many test flights. A quick summary of typical values can be found in Table 1, which is based on [13, 14]. Additionally, in static conditions there is no influence of rotor inertia on motor performance, so the propeller and motor selection can be decoupled, further simplifying the process.

Table 1: Typical applications for multirotors of different thrust-to-weight ratios.

Thrust-to-weight ratio	Application
2	Slow flight (minimum)
3	Payload transport; photography
4	Surveillance
5+	Aerobatics; high-speed video
7+	Racing

3.1.1. Propeller Sizing and Selection. The propeller sizing and selection process starts by defining a propeller database represented as a set of available propellers

$$\mathscr{P} := \{\mathbf{p}_i : i = 1, \ldots, n_p\}, \tag{2}$$

where the ith propeller $\mathbf{p}_i$ is defined by the pair

$$\mathbf{p}_i := (\mathbf{f}_{pi}, g_{pi}), \tag{3}$$

where $\mathbf{f}_{pi}$ denotes the ith propeller performance, which will be defined later, and g_{pi} denotes its physical properties expressed as a 4-tuple

$$g_{pi} := (d_i, \theta_{pi}, m_{pi}, s_{ni}), \tag{4}$$

where d_i is the ith propeller diameter, θ_{pi} is its pitch angle, m_{pi} is its mass, and s_{ni} is a discrete parameter representing the propeller series name. The propeller set $\mathscr{P}$ is then filtered to obtain a set of propellers $\mathscr{P}_p \subseteq \mathscr{P}$ that satisfy a requirement 4-tuple

$$g_{pr} = (d_{\min}, d_{\max}, m_{p_{\max}}, \mathscr{S}_{nr}), \tag{5}$$

where $d_{\min}$ is the minimum diameter, $d_{\max}$ is the maximum diameter, $m_{p_{\max}}$ is the maximum mass, and $\mathscr{S}_{nr}$ is a set of preferred series names

$$\mathscr{S}_{nr} := \{s_{nk} : k = 1, \ldots, n_s\}. \tag{6}$$

Thus

$$\mathscr{P}_p = \{\mathbf{p}_i : d_i \in [d_{\min}, d_{\max}], m_{pi} \in (0, m_{p_{\max}}], s_{ni} \in \mathscr{S}_{nr}\} \tag{7}$$

This helps save time when evaluating the performance data and calculating operating points that is done next.

The performance of the ith propeller $\mathbf{f}_{pi}$ is denoted as a triplet of bijective mappings

$$\mathbf{f}_{pi} := (\omega \mapsto T(\omega), \omega \mapsto \tau(\omega), \omega \mapsto P_p(\omega)), \tag{8}$$

where ω is the rotor speed, T is the thrust, τ is the torque, and P_p is the propeller power. Let $T_r^{(k)}$ denote a required thrust. For each $\mathbf{p}_i \in \mathscr{P}_p$, we determine a set of n_o operating points $o_{pi} = \{o_{pi}^{(k)} : k = 1, \ldots, n_o\}$ where

$$o_{pi}^{(k)} := (T_i^{(k)}, \omega_i^{(k)}, \tau_i^{(k)}, P_{pi}^{(k)}) \tag{9}$$

and where

$$T_i^{(k)} = T_r^{(k)}, \tag{10}$$

$$\omega_i^{(k)} = T^{-1}(T_r^{(k)}), \tag{11}$$

$$\tau_i^{(k)} = \tau(\omega_i^{(k)}), \tag{12}$$

$$P_{pi}^{(k)} = P_p(\omega_i^{(k)}). \tag{13}$$

An example of the mapping triplets for two propellers is shown in Figure 5 along with an illustration of obtaining o_{pi} from T_r.

Usually $n_o = 2$ operating points are calculated: the operating point at hover $o_{pi}^{(1)}$, and the Wide Open Throttle (WOT) operating point $o_{pi}^{(2)}$. These signify the lower and upper boundaries of the flight performance, respectively. A third operating point ($k = 3$) can also be defined that corresponds to the propeller limit speed designated by the manufacturer; this can be used for checking the feasibility of the other operating points. The thrust requirements, $T_r^{(1)}$ for the hover condition and $T_r^{(2)}$ for the WOT condition, can be calculated from

$$T_r^{(1)} = \frac{W_{\text{total}}}{n_{\text{rot}}}, \tag{14}$$

$$T_r^{(2)} = r_T \times T_r^{(1)}, \tag{15}$$

where W_{total} is the estimated total weight of the multirotor, n_{rot} is the number of rotors and r_T is the thrust-to-weight ratio. Except for the propeller (and motor) set filtering purposes, the methodology uses only the total estimated weight of the multirotor, as it is presumed that the frame, battery size, payload and control modules are preselected from the ones available to the user and suited for the application. As only static conditions are considered (multirotor inertia not considered), the weights of those components are of lower importance as opposed to the estimated weights of propellers, motors and ESCs, which are multiplied by the number of rotors

$$\begin{aligned} W_{\text{total}} = {} & n_{\text{rot}}(W_{\text{prop}} + W_{\text{motor}} + W_{\text{ESC}}) \\ & + W_{\text{frame}} + W_{\text{battery}} + W_{\text{payload}} + W_{\text{FC}} + W_{\text{other}}. \end{aligned} \tag{16}$$

In practice, due to the fact that the propeller characteristics mappings defined by (8) are often given in the form of sample points, interpolation must be used for the calculations. This introduces errors. Therefore, although in theory $P_p = \tau\omega$, often in practice (dependence on k removed for notational simplicity)

$$P_{pi} \neq \tau_i \omega_i, \tag{17}$$

hence an average of those two values is taken

$$P_{pi_{\text{avg}}} = \frac{1}{2}(P_{pi} + \tau_i \omega_i). \tag{18}$$

To choose the propeller, various selection criteria are available. If $n_o > 1$, then determining the minimum power solution is a

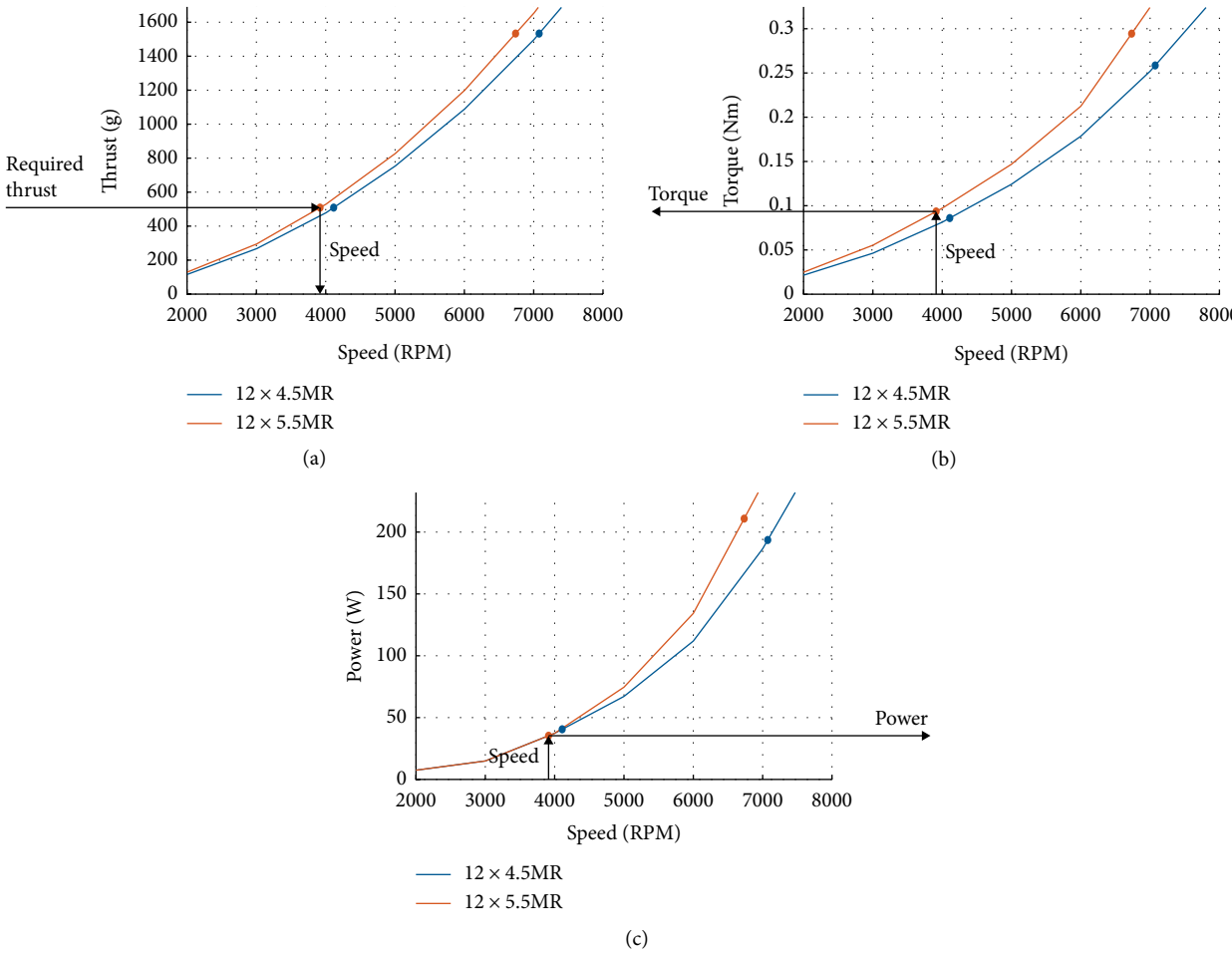


FIGURE 5: Example of obtaining a propeller operating point based on required thrust. (a) Obtaining speed from required thrust. (b) Obtaining torque from speed calculated in (a). (c) Obtaining power from speed calculated in (a).

multiobjective problem, and some user interaction is then helpful in making the selection. However, it is often possible to reduce the problem to the simplest case for $n_o = 1$, where the lowest power at hover operating point can be computed as follows

$$\mathbf{p}_{\text{selected}} := \arg\min_{\mathbf{p}_i \in \mathscr{P}_p} P^{(1)}_{pi_{\text{avg}}}. \tag{19}$$

In this case, the minimization can be quickly carried out through exhaustive search, thanks to the small set size due to the filtering in previous steps.

3.1.2. Motor Sizing and Selection. In a similar manner as for the propeller, let $\mathscr{M}$ be the set of available motors

$$\mathscr{M} := \left\{\mathbf{m}_j = \left(\mathbf{f}_{mj}, g_{mj}\right) : j = 1, \ldots, n_m\right\}, \tag{20}$$

where $\mathbf{f}_{mj}$ is the motor model described by the triplet of mappings

$$\mathbf{f}_{mj} := \left(I \mapsto P_m(I), I \mapsto P_e(I), \left(P_m, P_e\right) \mapsto \eta\left(P_m, P_e\right)\right), \tag{21}$$

where I is the current, P_m is the mechanical power, P_e is the electrical power, η is the efficiency and where g_{mj} denotes the motor properties expressed as a triplet

$$g_{mj} := \left(I_{\max_j}, \omega_{0j}, m_{mj}\right), \tag{22}$$

where $I_{\max_j}$ is the maximum allowable ith motor current, ω_{0j} is its maximum no-load speed and m_m is its mass.

Unlike the process for the propeller selection, the performances of the motors must be evaluated first. The required motor power is set to be $P_r = P^{(k)}_{p_{\text{selected}}}$. Then for each $\mathbf{m}_j \in \mathscr{M}$, we determine n_o motor operating point triplets

$$o^{(k)}_{mj} := \left(I^{(k)}_j, P^{(k)}_{ej}, \eta^{(k)}_j\right), \tag{23}$$

where (dependence on k removed for simplicity)

$$I_j = P_m^{-1}(P_r), \tag{24}$$

$$P_{ej} = P_e\left(I_j\right), \tag{25}$$

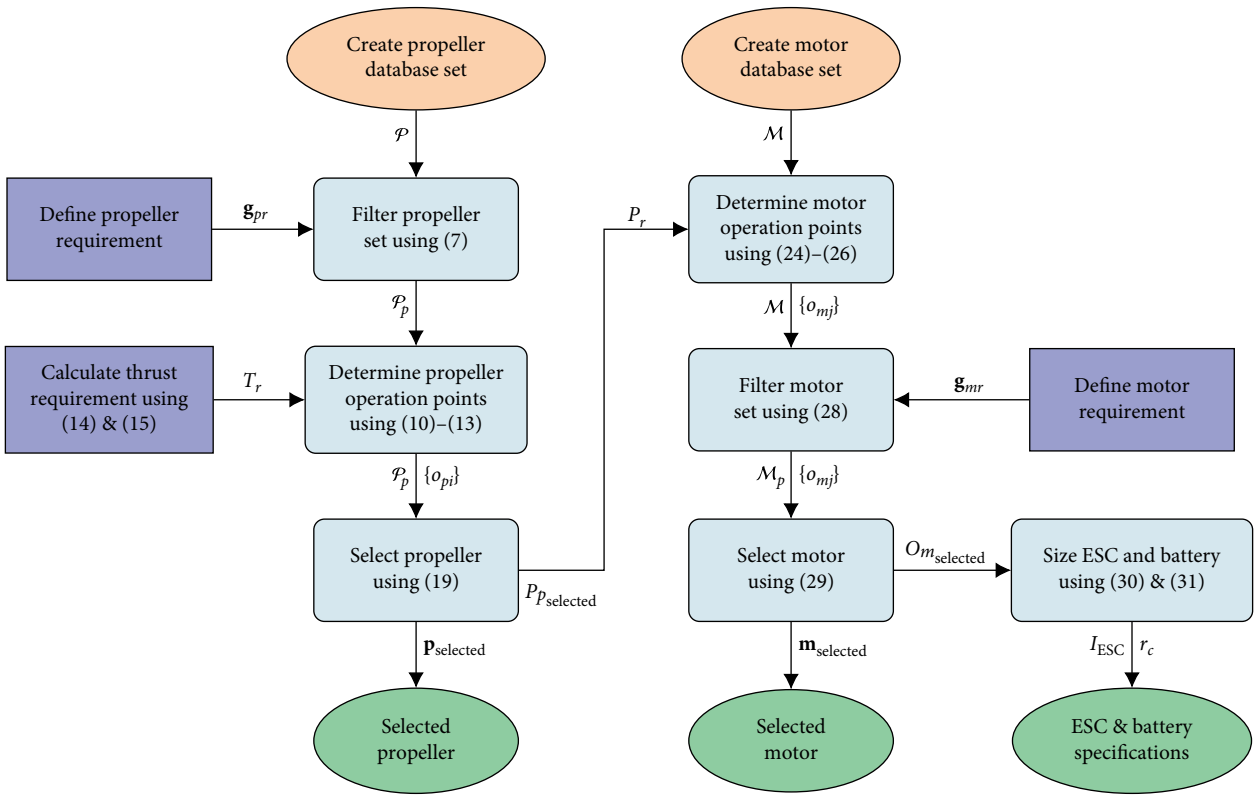


Figure 6: Actuating system sizing methodology information flow diagram.

$$\eta_j = \eta\left(P_r, P_{ej}\right). \tag{26}$$

It should be noted that the mapping $I \mapsto P_m(I)$ is not bijective in terms of motor characteristics, because at high current values most of the energy is dissipated as heat. However, considering the domain only up to the maximum current specified by manufacturer, the function is almost always monotonic. Therefore, in practice, over the domain $\left[0; I_{\max_j}\right]$ the inverse of power function P_m^{-1} can almost always be evaluated.

Knowledge of o_{mj} for all $\mathbf{m}_j \in \mathscr{M}$ allows for filtering of the motor set in regards to maximum current, speed and mass, thus obtaining $\mathscr{M}_p \subseteq \mathscr{M}$ that satisfies maximum current requirement on each motor $I_j \leq I_{\max_j}$ and a requirement pair

$$g_{mr} = \left(\omega_{\max}, m_{m_{\max}}\right), \tag{27}$$

where $\omega_{\max} = \omega^{(2)}_{\text{selected}}$ is the propeller speed at WOT and $m_{m_{\max}}$ is the maximum motor mass. Thus

$$\mathscr{M}_p = \left\{\mathbf{m}_j : I_j \leq I_{\max_j}, \omega_{0j} \geq \omega_{\max}, m_{mj} \leq m_{m_{\max}}\right\}. \tag{28}$$

Like in the propeller's case, various selection criteria could be used to choose the motor. In the simple example for $n_o = 1$ it could be the lowest electrical power

$$m_{\text{selected}} := \arg \min_{\mathbf{m}_j \in \mathscr{M}_p} P^{(1)}_{ej}. \tag{29}$$

Table 2: Data contained in sizing methodology outputs.

Output name	Data contained
Propeller specification	Name; diameter d; pitch θ_p; series s_n
Motor specification	Name; KV rating; rated speed $\omega^{(2)}_{\text{selected}}$; rated torque $\tau^{(2)}_{\text{selected}}$; rated mech. power $P^{(2)}_{m_{\text{selected}}}$; rated el. power $P^{(2)}_{e_{\text{selected}}}$; rated efficiency $\eta^{(2)}_{\text{selected}}$; nominal voltage V
ESC specification	Maximum current I_{ESC}
Battery specification	Cell number n_C; minimum C-rating r_C; capacity C

Again the filtering operation in (28) makes it possible to use exhaustive search for the minimization purpose.

3.1.3. ESC and Battery Sizing. The Electronic Speed Controller is sized mainly in regards to the maximum current it can handle. As it is assumed that the multirotor will never need more thrust than achieved at WOT operating point, the current should also not go over the calculated value. Therefore, it can be said that

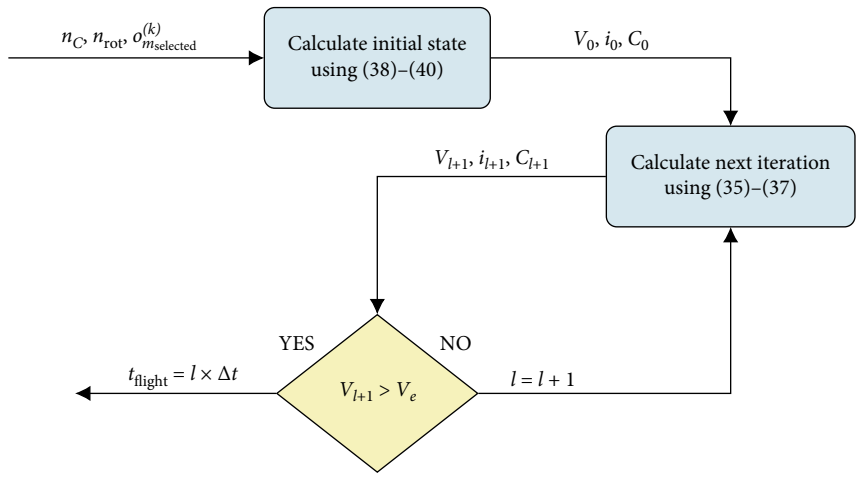


Figure 7: Power system calculation flowchart for kth operating point.

$$I_{ESC} = I^{(2)}_{selected}, \tag{30}$$

where I_{ESC} is the rated (maximal) ESC current and $I^{(2)}_{selected}$ is the motor current at WOT operating point.

A substantial part of battery specification needs to be provided by the user to realise flight time estimation as described in Section 3.2. However, the methodology allows to complete the battery specification by sizing the C-rating parameter

$$r_C = \frac{I_{ESC} \times n_{rot}}{C}, \tag{31}$$

where r_C is the minimal required battery C-rating and C is the battery capacity.

The whole actuating system sizing methodology is depicted by the data flow chart shown in Figure 6. It shows the dependence of motor sizing on propeller specification and ESC and battery sizing on motor specification. The light cyan blocks correspond to the methodology stages, the dark blue blocks show requirements and constraints and the orange ellipses signify points of database access. The output data in green ellipses include specification parameters for sizing all of the major components of the propulsion system (namely propeller, motor, ESC, and battery) and the calculated propeller and motor operating points that can be used for calculating additional data, such as estimated flight time. The data corresponding to each of the outputs can be found in Table 2.

In Figure 6, a substantial impact of estimated total drone weight can be also seen—it is used to calculate required thrust T_r that plays a key role in selecting the propeller, and consequently the motor. Due to the discrete nature of propeller and motor parameters, the relationship is highly nonlinear, so it needs to be analysed numerically. However, it is easy to implement the methodology in a loop to plot the characteristics of flight time versus weight, which may be used in a payload sizing application.

3.2. Power System. The power system section of the methodology focuses on flight time estimation by modelling the battery. The model is based on the iterative approach presented

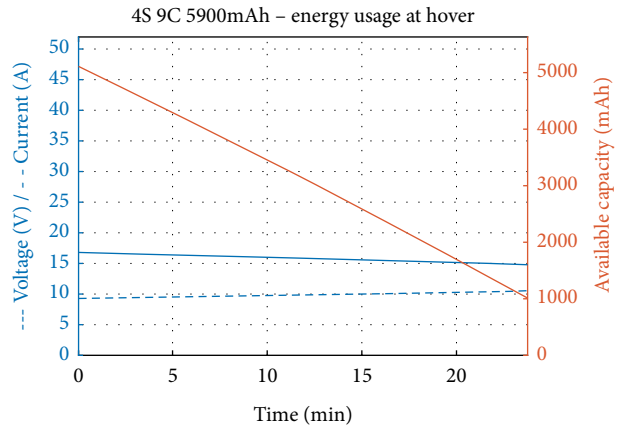


Figure 8: Example battery behaviour during hover.

by Traub [15]. It features two important phenomena—decrease of capacity with the increase of current and drop in voltage due to discharge. Additionally, the power demand can be varied throughout the simulation; however, in the base version of the methodology this is not used, as the operating points are constant. A block diagram of the calculations for one operating point can be seen in Figure 7.

Modelling of the battery capacity varying with drawn current is done through modified Peukert's equation in the form of:

$$t = \frac{Rt}{i^n}\left(\frac{C}{Rt}\right)^n, \tag{32}$$

where Rt is battery hour rating (1 hour in case of small packs) and n is Peukert's constant (1.3 for LiPo) dependent on battery type and temperature.

Measuring battery voltage is one of the main ways of measuring remaining charge in-flight. Typically, Lithium Polymer (LiPo) cells used in drones have 4.2 V when at full charge and drop to 3.7 V when at 20% charge. The voltage drop curve is nonlinear, but for the model it has been linearized and is expressed through

$$V(t) = V_0 - k_1[C_0 - C(t)], \tag{33}$$

Table 3: Errors between measured and simulated propeller characteristics—thrust coefficient (C_T) and power coefficient (C_P).

Mean C_T error	−0.0121
Mean relative C_T error	−12.6%
Mean std. deviation of C_T	0.0051
Mean C_P error	0.0059
Mean relative C_P error	2.48%
Mean std. deviation of C_P	0.0022

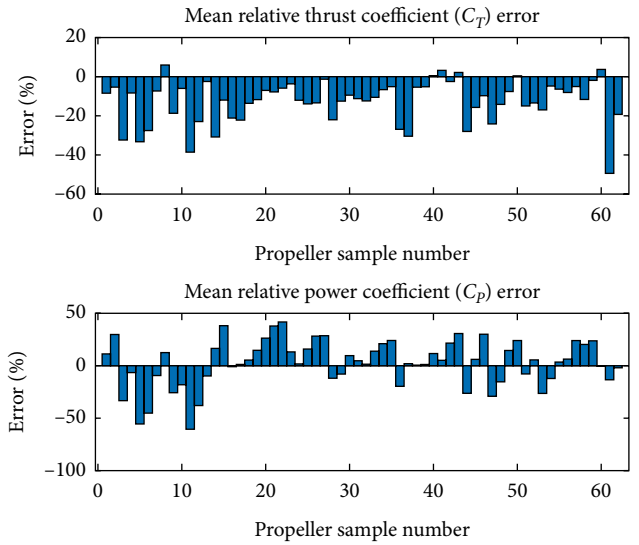


Figure 9: Relative errors between measured and simulated propeller coefficients.

$$k_1 = \frac{4.2\,\text{V} - 3.7\,\text{V}}{DoD \times C_0 \times n_C}, \tag{34}$$

where V_0 is the initial voltage, k_1 is the voltage drop coefficient, C_0 is the initial battery capacity, DoD is the maximal Depth of Discharge, and n_C is the number of battery cells. Based on Traub [15] the battery model can be defined with a set of iterative equations

$$V_{l+1} = V_0 - k_1[C_0 - C_l], \tag{35}$$

$$i_{l+1} = \frac{P_e}{V_{l+1}}, \tag{36}$$

$$C_{l+1} = i_{l+1}^{1-n} R t^{1-n} C^n - \sum_{m=1}^{l+1} i_m \Delta t \tag{37}$$

with the initial state defined as

$$V_0 = 4.2\,\text{V} \times n_C, \tag{38}$$

$$i_0 = \frac{P_e}{V_0}, \tag{39}$$

$$C_0 = i_0^{1-n} R t^{1-n} C^n. \tag{40}$$

The information flow in the model is visualized in Figure 7.

As time passes, the voltage decreases, therefore increasing current draw to achieve the same power, and consecutively decreasing available battery capacity due to Peukert's effect, as can be seen in Figure 8. The simulation is stopped when voltage reaches

$$V_e = 3.7\,\text{V} \times n_C \tag{41}$$

or when capacity reaches 20% of initial capacity (only works when power drawn is constant). The output is simply the simulation time, calculated as the product of the time step value and the number of iterations.

4. Example Results

The methodology presented has been implemented as a MATLAB script. This allows to easily process large quantities of data from propeller and motor databases and to plot component characteristics on every stage of the selection process.

In this example, performance data published by APC Propellers [16] will be used for the propeller database. It contains static and dynamic performance obtained through analytical methods of all products currently manufactured by the company. Due to the reliance on external computer software, airfoil drag (and consequently, torque) may be under-predicted at low speeds. Additionally, wind tunnel measurements of selected propellers [17] show overprediction of thrust coefficient (and consequently, thrust) of around 12% on average across all tested propellers. Detailed results are shown in Table 3 and in Figure 9. Therefore, an easily adjustable parameter called *Safety Factor* (*SF*) was introduced that increases required power at the WOT operating point to reduce the impact of mentioned inaccuracies and guarantee that the chosen motor will be able to reach the expected speed

$$I_j^{(2)} = P_m^{-1}(P_r \times SF), \tag{42}$$

$$\eta_j^{(2)} = \eta\left(P_r \times SF, P_{ej}\right). \tag{43}$$

There is no need to include *Safety Factor* in the ESC sizing, as the WOT operating point at which it is sized, in typical operating conditions, is achieved only for a few seconds at a time, not enough to damage the unit. The inclusion of the *Safety Factor* parameter in the battery sizing is recommended, as LiPo batteries are prone to ageing, which increases their internal resistance. Hence, with time at high currents more and more heat is generated, eventually leading to battery damage. What is more, cheap batteries are known for parameters varying between each unit, further justifying the need for an additional safety measure. Therefore, Equation (31) becomes

$$r_C = \frac{I_{\text{ESC}} \times n_{\text{rot}} \times SF}{C}. \tag{44}$$

For the motor database, a database bundled with Drive Calculator [2] software was used. It is based on measurements done and uploaded by its users, so it is impossible to accurately measure the discrepancies with real products, but they are estimated to be around 5–10% overall. However, a significant inaccuracy is introduced with the simplified motor model used

Table 4: Basic DJI Phantom 4 V2.0 parameters.

Number of rotors	4
Diagonal size	350 mm
Total weight	1375 g
Battery weight	468 g
Battery capacity	5870 mAh
Battery nominal voltage	15.2 V
Battery type	LiHV 4S
Propeller diameter	9 inch
Propeller pitch	5.5 inch

Table 5: Additional methodology parameters used in small drone sizing.

Thrust-to-weight ratio r_T	3
Min. propeller diameter $d_{\min}$	8 inch
Max. propeller diameter $d_{\max}$	9 inch
Safety Factor SF	1.05
Preferred propeller series $\mathscr{S}_{n_r}$	MR, E, E-3, E-4
Max. propeller mass m_{p_r}	24 g
Max. motor mass m_{m_r}	100 g

to calculate characteristics based on scarce data. The model, applicable both to BLDC and DC motors, considers only two sources of losses: copper losses, calculated using winding resistance

$$P_{\text{Cu}} = R_m I_{\text{motor}}^2 \tag{45}$$

and iron losses, calculated using no-load current

$$P_{\text{iron}} = V \times I_0, \tag{46}$$

where P_{Cu} are copper losses, R_m is the windings resistance (of all simultaneously working phases), I_{motor} is the current delivered to motor windings, P_{iron} are iron losses, V is the nominal voltage and I_0 is the no-load current. As the no-load measurement is usually done through an ESC, the iron losses also incorporate losses from the controller. The model, based on [18], is calculated as follows:

$$P_{\text{prop}} = \tau_{\text{prop}} \times \omega_{\text{prop}} \times SF, \tag{47}$$

$$I_{\text{motor}} = \frac{V - \sqrt{V^2 - 4R_m\left(P_{\text{iron}} + P_{\text{prop}}\right)}}{2R_m}, \tag{48}$$

$$P_{\text{motor}} = V \times I_{\text{motor}}, \tag{49}$$

$$\eta_{\text{motor}} = \frac{P_{\text{prop}}}{P_{\text{motor}}} \times 100\%, \tag{50}$$

where P_{prop}—is the power delivered to the propeller, τ_{prop} is the propeller torque, ω_{prop} is the propeller speed, P_{motor} is the motor electrical power, and η_{motor} is the motor efficiency.

To demonstrate the capabilities of the methodology a set of example results is presented for a low-weight drone. The results are validated against a similar commercial product. Based on the findings, a hypothetical usage of the methodology for sizing of Personal Air Vehicles is demonstrated.

4.1. Small Drone. For the ease of validation, the input parameters of the methodology were set to match those of the DJI Phantom 4 Pro V2.0, as indicated in Table 4. This enables easy comparison of the vehicle's published specification [19] with the sizing method's results in terms of flight time and propeller dimensions, as the manufacturer does not provide motor data. It should be noted here that the Phantom 4 uses LiHV (High Voltage LiPo) batteries rated at 3.8 V per cell, however in the calculations the more popular LiPo batteries, rated at 3.7 V per cell, are used. Additionally, V2.0 uses FOC-enabled drivers, which generate sinusoidal signals instead of the usual trapezoidal. However, the manufacturer advertises it as a means to reduce noise instead of improving performance, so it can be assumed that in this case the difference can be neglected.

The MATLAB script has been run considering two operating points: hover and WOT. The goal was to reduce energy usage at hover, as the platform's main purpose is photography. For the thrust the unit of gram-force (gf), which corresponds to the force acting on 1 gram of mass in a standard gravitational field, is used due to intuitiveness in this application. Additional sizing parameters are listed in Table 5. The results are below:

Results. For a 4-rotor drone with estimated AUM of 1375 g:

(i) APC 9×4.5E propeller should be chosen for the highest specific thrust of 9.69 gf/W per motor at hover.
(ii) Hacker B20 26L (2080 KV) motor should be selected with 0.15 Nm torque at maximum speed of 9600 RPM.
(iii) One motor uses 35 W of electrical power at hover and 237 W of electrical power at WOT.
(iv) The drive should be controlled by a 16 A ESC per motor.
(v) The whole system should be powered by a 4S 12C LiPo battery of 5870 mAh.
(vi) Hovering flight requires 124 W of mechanical power (0.05 Nm at 5600 RPM) to achieve 1375 gf of total thrust.
(vii) WOT flight requires 590 W of mechanical power (0.14 Nm at 9600 RPM) to achieve 4125 gf of total thrust.
(viii) This configuration should achieve around 26.9 min of hover and around 2.3 min of flight at WOT.

As can be seen, both the propeller and the motor were successfully selected and the estimated flight time has been calculated. The propeller is of lower pitch than in the reference drone, which might be explained by the unavailability of 9×5.5 propellers in APC's range, and 9×6 being too power-consuming. Especially interesting is the choice of E-series (electric airplanes) propeller over MR-series (multirotors),

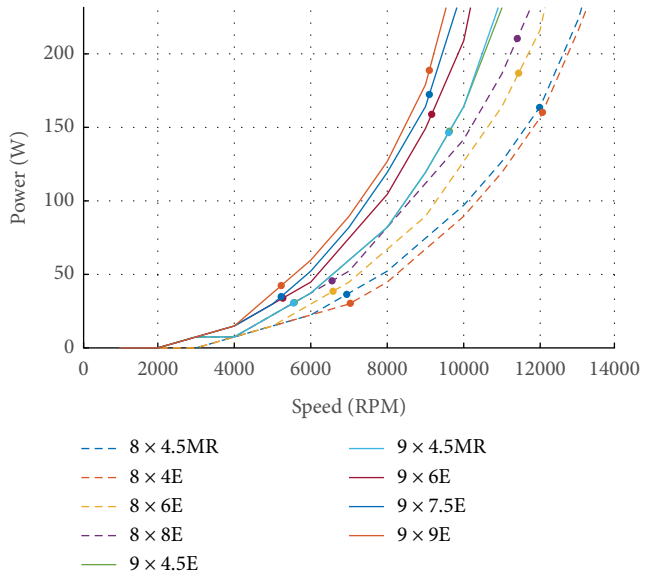


Figure 10: Comparison of power–speed characteristics of 8 and 9 inch propellers.

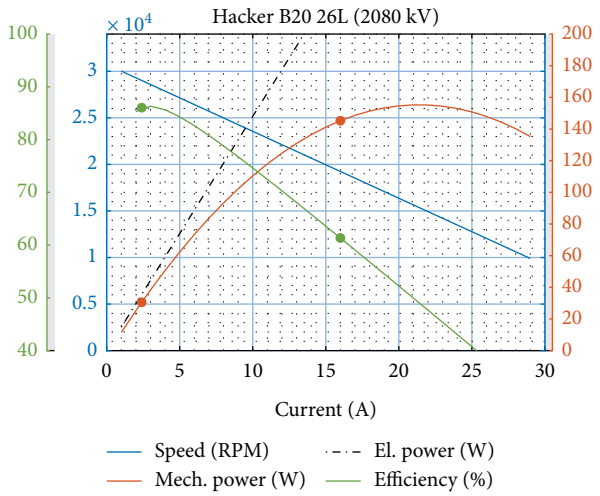


Figure 11: Simulated operating characteristics of Hacker B20 26L brushless motor.

which can be influenced by numerical errors due to interpolation, specifically at low speeds required for hovering. Comparison of power characteristics of propellers considered in this example can be seen in Figure 10.

Hacker B20 26L is a surprising choice for the application, as it is an inrunner motor that usually comes with gearing to increase its torque for traction applications. However, in this case it is used in direct drive configuration, which is possible due to the low speed of a large propeller. Its measured KV is 2080 (as opposed to 2020 stated by the manufacturer [20]), which puts the hover operating point almost at the maximum of the efficiency curve, therefore increasing the flight time, as can be seen in Figure 11.

The calculated flight time seems to be in line with the achievements of the reference drone. Maximum flight time

Table 6: Drone parameters used in further testing.

Name	GTQ Mini [8]	IRIS+ [21, 24]	PD6-AW2 BASIC [25]	Fox 4 [26]
Take-off mass [kg]	0.5	1.3	10	4
Thrust-to-weight ratio	2	2.6	3.5	2.5
Rotor count	4	4	6	4
Min. propeller diameter [inch]	3	8	18	10
Max. propeller diameter [inch]	5	10	21	15
Battery cell count	4	3	6	6
Battery capacity [mAh]	850	5100	2×16000	2×5000

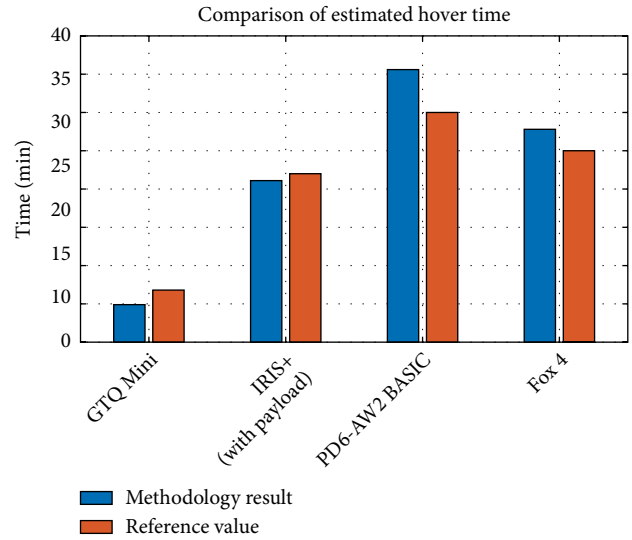


Figure 12: Comparison of calculated hovering time with longest expected time.

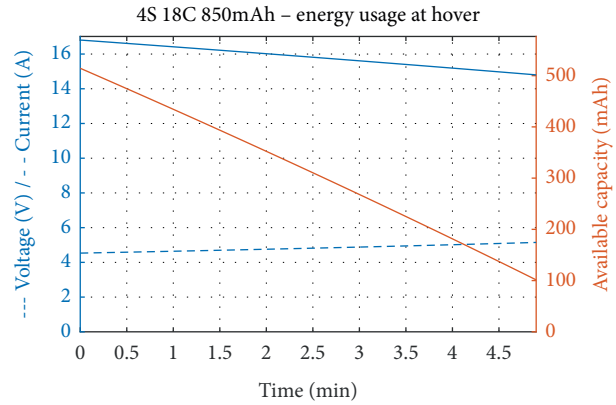


Figure 13: Battery behaviour of GTQ Mini during hover.

stated by the manufacturer is 30 min [19], but it was probably measured in flight at best endurance speed, which uses slightly less power than in hover ([21]) due to the reduction of the

Table 7: Uses of sizing methodology based on data available.

Propeller data	Motor data	Example uses
Available	Available	Complete sizing of multirotor propulsion system; flight time estimation; optimisation of flight time
Available	Not available	Propeller sizing; preliminary motor design
Not available	Available	Battery and ESC sizing; flight time estimation
Not available	Not available	—

induced drag. Therefore, it can be assumed that the maximum hover time will be close to the 27 min calculated, which seems to be confirmed by independent tests achieving 23–26 min of hover [22, 23]. However, as the calculations do not include dynamic effects of flight, the prediction accuracy for the WOT operating point is considerably lower. Furthermore, that point is set arbitrarily based on thrust-to-weight ratio, and is rarely measured in real operation, so no validation could be performed.

The reference drone is a commercially popular product, therefore it can be assumed that its performance is close to optimal for its given weight and application (aerial photography). Therefore, achieving results of similar value to the reference may indicate that the chosen configuration has performance close to optimal. Considering the accuracy of results, the assumptions and estimations used and the low computational cost, methodology performance can be considered satisfactory for applications in other research projects and on its own.

4.2. Further Validation. In similar manner to validation through comparison with DJI Phantom 4 v2.0, more tests of different configurations were conducted. The input parameters are summarised in Table 6. 6S batteries were assumed for Fox 4 and PD6-AW2 BASIC platforms, as those are more suited for the heavy lifting application. The weight of IRIS+ is taken with a sample payload. Thrust-to-weight ratio was adjusted so if more payload was added up to maximum allowable mass, the drone would still maintain controllability with thrust-to-weight ratio of 2. In 3 of the test cases, results shown in Figure 12 seem to be in satisfactory agreement with the manufacturer's specification considering that the methodology does not include the power usage by the flight controller, sensors, RC communication or payload.

The significant difference in the case of GTQ Mini needs to be addressed separately. The methodology has returned similar results to those of the methodology presented by Bershadsky et al. [8]. Our methodology has chosen 5×4.3 propellers as compared to 5×3, 1378 KV motor as compared to 1383 KV and uses 4.54 A in hover (at full battery) as compared to 4.49 A. However, there is a 1.9 min difference in calculated hover times. With the same battery capacity and similar current drawn, the discrepancy might be that in [8] the simulation is stopped when battery reaches 3.6 V, while our implementation is set up to stop earlier at 3.7 V. Another difference is probably in the battery model used, as our methodology simulates the decrease of voltage with discharge, leading to the increase in current drawn from 4.54 A to 5.15 A throughout battery operation, as can be seen in Figure 13.

4.3. Personal Air Vehicle. The current implementation of the methodology as a MATLAB script does not allow the sizing of heavy platforms, such as PAV, due to the lack of a sufficiently large propeller in database. However, the methodology can be implemented with different databases and even modified to help with the design of components: propeller specification provides enough data for presizing of an electric motor, and thrust requirements along with size and weight constraints can be used as input in propeller design. Additionally, using only scarce data, a flight time estimation can be performed to validate the design of components. This is an especially important feature, as the methodology has been designed with the ability to be used inside another algorithm to further enhance the optimisation process. That way questions, such as rotor number, propeller, size or maximum payload, can be answered. This is especially important for PAV, where the mass constraint is very tight because of the payload in the form of a passenger. Table 7 outlines example uses of the methodology in scenarios with different data available.

Some of the problems of Personal Air Vehicles, such as high weight of the platform, can be addressed by alternative multirotor designs. Papa [27] discusses a multirotor in which a part of the lifting is done by a balloon. Our methodology is simple and flexible enough to complement the approach in [27]. Papa's method can be used for sizing the balloon while our methodology sizes the multirotor part by subtracting the calculated balloon's lift from the estimated platform's weight and using it as an input. Validation of this approach, however, needs to be performed.

5. Conclusion

The methodology presented in this paper answers the need to have an automated process of selecting multirotor components using a simple input of estimated drone weight. Validation was performed using data from four commercially available multirotors (including DJI Phantom 4 V2.0) and one specialised platform, which shows that the obtained results are in accordance with manufacturer data and independent tests.

The simplicity and open-loop approach are also the limitations of this methodology. The use of static model does not provide enough information to estimate the acceleration, turn speed or performance in wind conditions. However, the inclusion of a dynamic model would require the bandwidth limitations of the actuators to be considered. This would overly increase the complexity of the methodology and would demand much more input data, thus limiting the usability.

Although there are no conceptual constraints preventing the use of the methodology for sizing large passenger multirotors, considerable limitations are introduced by the

databases used, which rarely provide data on large propellers in the 50–60 inch range and motors able to support them. However, it is assumed, that certain elements of the methodology, such as flight time estimation based on limited data, can be useful in the process of PAV design. Finally, the proposed methodology is also flexible enough to accept data of custom designed components or to be used for sizing of certain alternative multirotor topologies.

Unfortunately, one of the most important disadvantages of this methodology is its low, hard to estimate, accuracy. Great care was taken to make the results as close to reality as possible, but due to assumptions made for the sake of simplicity and speed, such as the use of thrust-to-weight ratio instead of calculation of maximum required thrust, the accuracy of calculations is impossible to measure. If needed, it can be enhanced, for example by improving motor model or using databases with only measured data, but it is advised against relying on the results in safety-critical applications.

Data Availability

The MATLAB code used to support the findings of this study have been deposited in the GitHub repository (https://github.com/mbiczyski/Multirotor-Sizing-Methodology). APC propeller performance data used to support this study is available at https://www.apcprop.com/technical-information/performance-data/. These datasets are cited at relevant places within the text as reference [12]. Previously reported propeller experimental performance data were used to support this study and are available at http://m-selig.ae.illinois.edu/props/propDB.html. These prior studies (and datasets) are cited at relevant places within the text as reference [14]. Motor performance data used to support this study is available at http://www.drivecalc.de/. These datasets are cited at relevant places within the text as reference [3].

Conflicts of Interest

The authors declare that there have no conflicts of interest.

Funding

Research and publication of the article was funded by ESTACA, France, and Cranfield University, UK.

References

[1] G. Szafranski, R. Czyba, and M. Blachuta, "Modeling and identification of electric propulsion system for multirotor unmanned aerial vehicle design," in *2014 International Conference on Unmanned Aircraft Systems*, pp. 470–476, IEEE, Orlando, FL, USA, 2014, ICUAS 2014 - Conference Proceedings.

[2] C. Persson, "Drive calculator," 2019, http://www.drivecalc.de/.

[3] Solution for All Markus Müller, "eCalc - the most reliable electric motor calculator on the web for RC pilots," 2019, https://www.ecalc.ch/

[4] M. Gatti and F. Giulietti, "Preliminary design analysis methodology for electric multirotor," *International Federation of Automatic Control Proceedings Volumes*, vol. 46, no. 30, pp. 58–63, 2013.

[5] M. Gatti, "Complete preliminary design methodology for electric multirotor," *Journal of Aerospace Engineering*, vol. 30, no. 5, p. 9, 2017.

[6] M. Kim, H. Joo, and B. Jang, "Conceptual multicopter sizing and performance analysis via component database," in *2017 Ninth International Conference on Ubiquitous and Future Networks (ICUFN)*, vol. 7, pp. 105–109, IEEE, Milan, Italy, 2017.

[7] P. M. Basset, A. Tremolet, and T. Lefebvre, "Rotary wing UAV pre-sizing : past and present methodological approaches at Onera," *Aerospace Lab*, vol. 8, pp. 1–12, 2014.

[8] D. Bershadsky, S. Haviland, and E. N. Johnson, "Electric multirotor UAV propulsion system sizing for performance prediction and design optimization," in *57th AIAA/ASCE/AHS/ASC Structures, Structural Dynamics, and Materials Conference*, vol. 1, pp. 1–22, American Institute of Aeronautics and Astronautics, Reston, Virginia, 2016.

[9] X. Dai, Q. Quan, J. Ren, and K.-Y. Cai, "An analytical design-optimization method for electric propulsion systems of multicopter UAVs with desired hovering endurance," *IEEE/ASME Transactions on Mechatronics*, vol. 24, no. 1, pp. 228–239, 2019.

[10] X. Dai, Q. Quan, J. Ren, and K.-Y. Cai, "Efficiency optimization and component selection for propulsion systems of electric multicopters," *IEEE Transactions on Industrial Electronics*, vol. 66, no. 10, pp. 7800–7809, 2019.

[11] O. Magnussen, M. Ottestad, and G. Hovland, "Multicopter design optimization and validation," *Modeling, Identification and Control*, vol. 36, no. 2, pp. 67–79, 2015.

[12] J. M. Miller, "Energy storage technologies," *Propulsion Systems for Hybrid Vehicles*, pp. 439–522, Institution of Engineering and Technology, 2010, chapter 10.

[13] Half Chrome Drones, "Drone thrust testing," 2019, https://www.halfchrome.com/drone-thrust-testing/.

[14] O. Liang, "How to choose motor for racing drone & quadcopter," 2019, https://oscarliang.com/quadcopter-motor-propeller/.

[15] L. W. Traub, "Range and endurance estimates for battery-powered aircraft," *Journal of Aircraft*, vol. 48, no. 2, pp. 703–707, 2011.

[16] APC Propellers, "Performance data," 2019, https://www.apcprop.com/technical-information/performance-data/.

[17] J. B. Brandt, R. W. Deters, G. K. Ananda, and M. S. Selig, "UIUC propeller database," 2019, http://m-selig.ae.illinois.edu/props/propDB.html.

[18] Radio Control Info, "Brushless motor efficiency and constants," http://www.radiocontrolinfo.com/brushless-motor-efficiency/

[19] DJI, "DJI Phantom 4 Pro V2.0.," 2019, https://www.dji.com/phantom-4-pro-v2.

[20] Hacker, "B20 26 L kv2020 + 4:1," https://www.hacker-motor-shop.com/Brushless-Motors/Hacker-Inrunner/Hacker-B20/B20-L-with-Gears/B20-26-L-kv2020-4-1.htm?shop=hacker_e&SessionId=&a=article&ProdNr=10017700&p=2072&rdeocl=1&rdetpl=categorypage&rdebox=box4/.

[21] C. Di Franco and G. Buttazzo, "Energy-aware coverage path planning of UAVs," in *2015 IEEE International Conference on Autonomous Robot Systems and Competitions*, pp. 111–117, IEEE, Vila Real, Portugal, 2015.

[22] T. Luna, "DJI Mavic 2 Pro vs. Phantom 4 Pro v2.0!," 2018, May 2019, https://www.wetalkuav.com/dji-mavic-2-pro-vs-phantom-4-pro-v2-0/.

[23] K. Smith, "DJI Mavic Pro VS Phantom 4 Pro V2. 0: which drone is better?" 2018, May 2019, https://myfirstdrone.com/blog/dji-mavic-pro-vs-phantom-4-pro-drone-better/.

[24] Arducopter, "Iris RTF quadcopter UAV support - Arduino based Arducopter UAV, the open source multi-rotor," 2019, September 2019, http://www.arducopter.co.uk/support.html.

[25] Prodrone, "PD6-AW2 BASIC," September 2019, https://www.prodrone.com/products/pd6-aw2-basic/.

[26] Hélicéo, "Multirotor drone for professionals, surveyors & topographers Fox4," 2019.September 2019, http: //www.heliceo.com/en/produits-pour-geometres/fox4-multirotor-drone/.

[27] U. Papa, *Embedded Platforms for UAS Landing Path and Obstacle Detection*, vol. 136 of *Studies in Systems Decision and Control*, Springer International Publishing, 2018, cham.



https://dspace.org/

Multirotor sizing methodology with flight time estimation

Biczyski, Marcin; Sehab, Rabia; Whidborne, James F.; Krebs, Guillaume; Luk, Patrick Chi-Kwong

2020-01-20
Wiley/Hindawi
https://doi.org/10.1155/2020/9689604
Biczyski M, Sehab R, Whidborne JF, et al., (2020) Multirotor sizing methodology with flight time estimation. Journal of Advanced Transportation, Volume 2020, Article number 9689604

Downloaded from a DSpace repository. https://dspace.org/